Available online at www.sciencedirect.com
ScienceDirect
Journal of the European Ceramic Society 29 (2009) 801–811
www.elsevier.com/locate/jeurceramsoc

Understanding the mechanical properties of hot pressed Ba-doped S-phase SiAlON ceramics

Bikramjit Basu [a,*], Manisha [a], N.K. Mukhopadhyay [b]

[a] *Laboratory for Advanced Ceramics, Department of Materials and Metallurgical Engineering, Indian Institute of Technology Kanpur (IIT-Kanpur), India*
[b] *Center for Advanced Studies, Department of Metallurgical Engineering, Institute of Technology, Banaras Hindu University, Varanasi 221005, India*

Received 20 March 2008; received in revised form 4 July 2008; accepted 9 July 2008
Available online 9 August 2008

Abstract

In this contribution, we report the analysis and interpretation of the mechanical property measurements for a new class of SiAlON ceramic. The hardness and indentation fracture toughness were measured on the hot pressed Ba-doped S-SiAlON ceramic using Vickers indentation at varying loads (up to 300 N). An important observation was that all the investigated S-SiAlON exhibited the characteristic rising R-curve behavior with a maximum toughness of up to 10–12 MPa $m^{1/2}$ for ceramics, hot pressed both at 1700 and 1750 °C. Crack deflection by large elongated S-phase grains and crack bridging by β-Si_3N_4 needles has been found to be the major toughening mechanisms for the observed high toughness. Theoretical estimates, using a toughening model based on crack bridging and deflection by platelet shaped 'S'-phase grains and β-Si_3N_4 needles, reveal the interfacial friction of around 200 MPa. Careful analysis of the indentation data reveals the average (apparent) hardness modestly increases with indent load in all S-SiAlON samples, with more significant effect for S-SiAlON, hot pressed at 1600 °C. This effect has been analyzed in the light of the established model of 'indentation-induced cracking' phenomenon. Our experimental results suggest that a modest combination of average hardness of 15 GPa and indentation toughness of around 12 MPa $m^{1/2}$ could be achieved in Ba-S-SiAlON ceramic and further improvement requires microstructural tailoring.

Keywords: Hot pressing; Mechanical properties; Hardness; Platelets; Si_3N_4

1. Introduction

In last few decades, silicon nitride (Si_3N_4)-based ceramics have been developed as the potential candidate for various engineering applications, such as cutting tool inserts, valve seals, seal rings, cylinder liners as well as in a variety of structural components for high efficiency engines and other mechanical systems.[1] Among silicon nitride-based ceramics, SiAlON ceramics, in particular, have been widely researched for structural applications because of the relative ease of fabrication and high oxidation resistance.[1–8] The solid solutions of α-Si_3N_4 and β-Si_3N_4 with Al and O are widely known as α-SiAlON and β-SiAlON, respectively. Depending on the extent of replacement of *m*(Si–N) bonds by *m*(Al–N) bonds and *n*(Si–N) bonds by *n*(Al–O) bonds; theses two variants (α- and β-SiAlON) have quite distinct properties. Of these two variants, α-SiAlON ceramic is nearly single phase ceramic with a better thermal shock resistance, chemical stability, and high hardness over a wide temperature range. This coupled with the lower density (3.2 gm/cm^3) have made these materials to be considered as a potential candidate for bearing applications. However, the lower strength and fracture toughness have proved as a bottleneck for their successful applications. Among the various approaches attempted, "*single phase in situ toughened α-SiAlON*" has been reported to exhibit an optimized combination of mechanical properties, in particular hardness and fracture toughness.[9–14] Interestingly, a recent research paper reports good cell adhesion property of rare-earth oxide-doped SiAlON ceramics, indicating the possible biomedical applications of SiAlON materials.[7] It may be pointed out here that an optimal combination of hardness, toughness, elastic modulus and strength are desired for load-bearing implants.

In recent times, Ba/Sr-doped S-phase SiAlON ceramics have received limited attention.[15–17] In an earlier work, we have reported the microstructural development and phase assemblage

* Corresponding author. Tel.: +91 512 2597771; fax: +91 512 2597505/259007.
E-mail address: bikram@iitk.ac.in (B. Basu).

0955-2219/$ – see front matter © 2008 Elsevier Ltd. All rights reserved.
doi:10.1016/j.jeurceramsoc.2008.07.005

study of the Ba-doped S-SiAlON ceramic[17] and in this follow-up work, the same hot pressed samples are investigated for detailed mechanical property evaluation. The transmission electron microscopy (TEM) analysis of the hot pressed microstructure, revealed the complex microstructure, consisting of major amount of coarser, tabular-shaped 'S-phase' grains as well as noticeable amount of β-Si_3N_4 needles and residual glassy phase.[17] In order to obtain an understanding of the basic mechanical behavior of such a new SiAlON composition, we have performed systematic indentation measurements at various loads. While the mechanical properties of various compositionally tailored/modified SiAlON ceramics (α- and β-SiAlON) are widely reported, it is of our interest to investigate whether the characteristic coarser elongated 'S' phase morphology in Ba-doped S-SiAlON ceramic can provide better toughness. A major focus in the present work is therefore to establish microstructure–mechanical property relationship of a rather new SiAlON system. In addition, it is of importance to see how S-SiAlON ceramic competes with other candidate SiAlON ceramics, in terms of overall mechanical properties. The present study is therefore of relevance for future research as how processing and microstructure can be refined to further improve properties of S-SiAlON material. It needs to be critically pointed out here that the mechanical property Ba-containing S-SiAlON ceramic has not been investigated to a greater extent and all the above aspects therefore establish the novelty of the present work.

2. Experimental procedure

The starting powders were the high purity commercial powders of $BaCO_3$ (Aldrich, UK), Si_3N_4 (UBE Grade SNE10, Japan), AlN (Starck grade C, Germany) and Al_2O_3 (Alcoa, USA). Appropriate amount of the precursor powders with a targeted S-phase composition of $BaAlSi_5O_2N_7$ were ball-milled in Si_3N_4 media for 24 h using isopropyl alcohol. The dried powder mixture was subsequently hot pressed at 30 MPa pressure in BN-coated graphite dies using RF heating in the temperature range of 1600–1750 °C for 2 h in nitrogen atmosphere. Three of the materials thus fabricated are (a) S-SiAlON, hot pressed at 1600 °C (S1600), (b) S-SiAlON, hot pressed at 1700 °C (S1700) and (c) S-SiAlON, hot pressed at 1750 °C (S1750). The density of hot-pressed specimens is measured by Archimedes's principle in water. For the mechanical property measurements, the optically reflective surfaces were obtained through standard ceramographic sample preparation technique. The elastic modulus was measured using the ultrasonic pulse-echo technique, which involves the sound wave velocity measurement in the solid. To assess the reproducibility of velocity measurement, the ultrasonic probe was placed at various locations on the surface of the hot pressed disc to acquire the flight time of the ultrasonic wave and an average of at least five readings were considered while computing ultrasound wave velocity.

Microstructural characterization was performed using scanning electron microscope (SEM) (Quanta FEI 200, The Netherlands) with attached energy dispersive spectroscopy (EDS) and transmission electron microscope (TEM) (JEOL 2000 FX). The electron transparent thin foil of S1700 sample for TEM investigation was prepared by the standard preparation route, which involves grinding, polishing followed by ion milling using Ar^+ ions. The mechanical properties, in particular hardness and indentation fracture toughness of S-SiAlON materials have been determined by indenting the mirror polished surfaces at varying loads of 100, 200, and 300 N for a dwell time of 15 s using Vickers Hardness Tester (Model-MVM 50). It can be noted that the hardness and toughness values for 50 N indent load have been taken from Ref. 17. Such a selection of indent loads (50–300 N) has been made in order to study indentation size effect. In addition, as far as the choice of macro-load in contrast to micro-load is concerned, it needs to be mentioned that the sintered microstructure of Ba-S-SiAlON is rather complex, containing the characteristic coarse-grained platelet-shaped S-phase, residual glass and acicular β-Si_3N_4. Therefore, the mechanical response of such a combination of microstructural phases requires large indentation size. It should be emphasized that the use of microhardness would cause a large variation in hardness property of such a material (depending on the location of indents). In fact, Krell clearly pointed out that the use of micro-loads needs to be avoided for evaluating hardness properties of various structural ceramics with complex microstructures.[18]

The fracture toughness (K_{Ic}) has been evaluated using the indentation fracture (IF) toughness technique. In the present work, the indentation fracture toughness K_{Ic} (MPa $m^{1/2}$) has been calculated using the appropriate formula proposed by Niihara et al.[19] for median cracks ($l/a \geq 1.5$):

$$K_{Ic} = 0.0667(l + a)^{-3/2} \times P \times \left(\frac{E}{H}\right)^{2/5} \quad (1a)$$

However, for the Palmqvist type of crack ($0.25 \leq l/a \leq 2.5$), a different formulation is used,[20]

$$K_{IC} = \frac{0.0181\ P(E/H)^{2/5}}{\sqrt{l}a} \quad (1b)$$

where P is indentation load (N), $2a$ is the average indent diagonal length (μm), $2c$ is the crack length (from one crack tip to another) and l is the difference of c and a (μm), E is the elastic modulus (GPa) and H is the hardness (GPa).

Both the indent diagonal and crack length are carefully measured from SEM images of the indented surfaces and the reported hardness and fracture toughness values are the average of at least five indentation measurements.

3. Results

3.1. Microstructural characterization

The microstructural characterization of hot pressed S-SiAlON ceramics has been carried out using both scanning electron microscopy (SEM) and transmission electron microscopy (TEM). XRD results indicated the predominant presence of S-phase with the detectable amount of β-Si_3N_4 and in some samples unreacted α-Si_3N_4 (not shown here and reported in

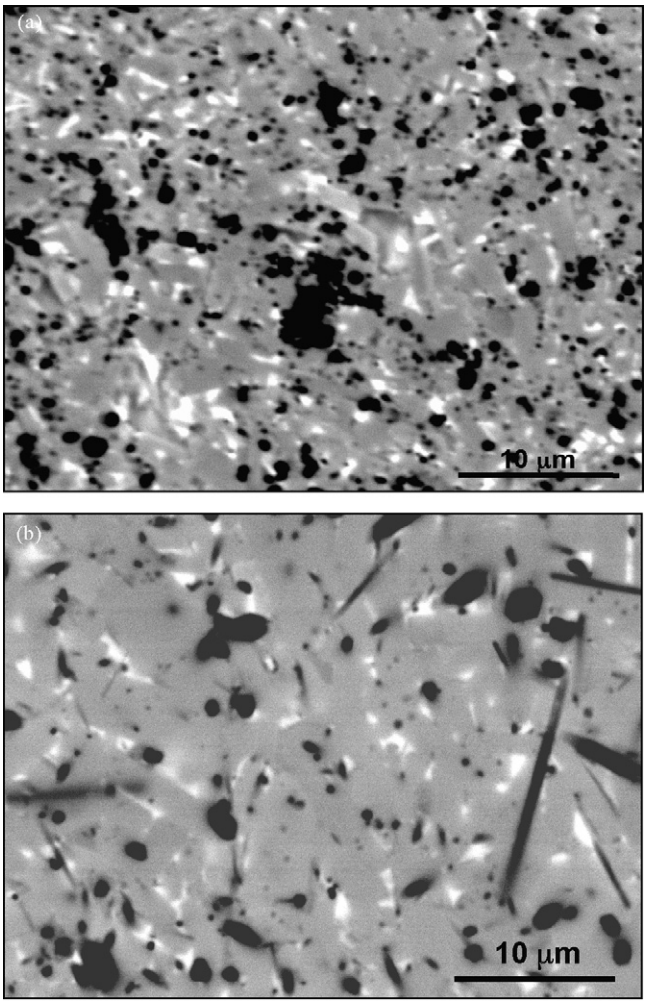

Fig. 1. Scanning electron micrograph (SEM) images (BSE mode) of S-SiAlON, hot pressed at (a)1600 °C and (b)1750 °C, respectively. Various microstructural phases can be distinguished as, S-SiAlON (grey), darker/black: unreacted Si_3N_4 in (a) and β-Si_3N_4 in (b). The bright contrast phase is residual glass phase.

Ref. 17). The representative SEM images (BSE mode) of S1600 and S1750 are provided in Fig. 1(a) and (b), respectively. The three characteristic microstructural phases of the investigated ceramic include: (a) S-phase with coarse elongated morphology (gray contrast), (b) β-Si_3N_4 with characteristic acicular (rod-like) morphology (darker contrast) and (c) traces of intercrystalline glassy residue (bright contrast). The quantification of the amount of various phases has been performed using commercial image analysis software. It was found that S1700 ceramic is characterized by nearly 85% coarse elongated S-phase, 7–9% β-Si_3N_4 needles and 6–8% glassy phase. In case of S1600 sample, higher amount of residue glass (12–15%) and more than 10% unreacted α-Si_3N_4 phase was measured. Much less amount of glass (2–4%) is however recorded in S1750 sample. Compared to S1600 samples, S1750 ceramic exhibited more fully developed elongated S-phase grains and acicular β-Si_3N_4 along with the reduced amount of the glassy phase at triple points (Fig. 1a). This difference in the relative development of the two constitutive phases might be ascribed to higher processing temperature, as has already been reported by Mitomo and Uenosono.[21]

TEM investigation of the selected S1700 sample was carried out to reveal the finer scale microstructure (see Fig. 2). In Fig. 2a, the characteristic tabular-shaped S-phase grains, oriented in different directions can be clearly observed. Also, can be noted is the presence of β-Si_3N_4 particulates in the S-phase, suggesting these to be acting as the heterogeneous nucleating sites for S-phase. As reported in Ref. 17, the average S-phase composition, based on multiple TEM-EDS analysis, can be confirmed as $Ba_2Si_{12-x}Al_xO_{2+x}N_{16-x}$ ($x = 2.0 \pm 0.2$). TEM-EDS analysis reveals the presence of Ba-rich aluminosilicate as residue glass phase at the grain boundary triple pockets (Fig. 2a). From multiple bright field TEM images of a thin section of S1700 ceramic, at least 20 grains of S-phase were considered for quantification of microstructural parameters. Such an analysis reveals that the aspect ratio of S-phase grains vary in the range of 3.1–4.3, with the average value of 3.4. The width of S-phase grains (minor axis) lies in the range of 0.6–1.4 μm, while the length (major axis) varies between 1–5 μm. For the analysis of β-Si_3N_4 sizes, a number of SEM images were used and more than 25 β-needles were measured. The average width and aspect ratio of β-Si_3N_4 needles were recorded as 0.57 μm and 7, respectively. In Fig. 2b, the observation of a typical acicular β-Si_3N_4 phase, with an aspect ratio of 7–8, can be made. More detailed microstructural characterization has been reported in our previous work.[17]

3.2. Mechanical characterization

The mechanical properties, in particular hardness and fracture toughness of the material were evaluated through the Vickers indentation technique at varying loads of 100–300 N. In order to study the indentation cracking behavior of S-SiAlON ceramics, SEM analysis of the Vickers indents was carried out. Both indent diagonals and crack lengths around the indentations were measured from the SEM images. Some representative SEM images of the indented SiAlON surfaces (S1750 sample) are provided in Fig. 3. At all the selected indent loads, the Vickers indentations were recorded to be sharp and even at 300 N indent load, no spalling and/or bulging around the indent edges were observed. Such observations indicate better damage tolerance property, as severe spalling around indentation at such high load is commonly reported for classical brittle material, like Al_2O_3 or glass–ceramics. A high magnification SEM image, showing the entire indent image (Fig. 3a), reveals the absence of any significant cracking at indent edges. Fig. 3b clearly demonstrates the well-developed radial-median crack morphology and in most cases, multiple cracking from single indent corner is not observed. Careful measurements of the indent diagonal length (a), crack length (l) are measured from multiple SEM images of at least five indents (at a given indent load) and the measured data as well as l/a ratio are summarized in Table 1. The computed hardness and toughness values are presented in Table 2. The toughness values are computed according to Eq. (1a) and the hardness or toughness values for 50 N indent load are taken from Ref. 17 In Table 2, the pulse-echo measured elastic modulus (E) values of the investigated S-SiAlON materials are also provided. The longitudinal sound wave velocity across the thickness of the hot pressed discs was recorded to vary in the range

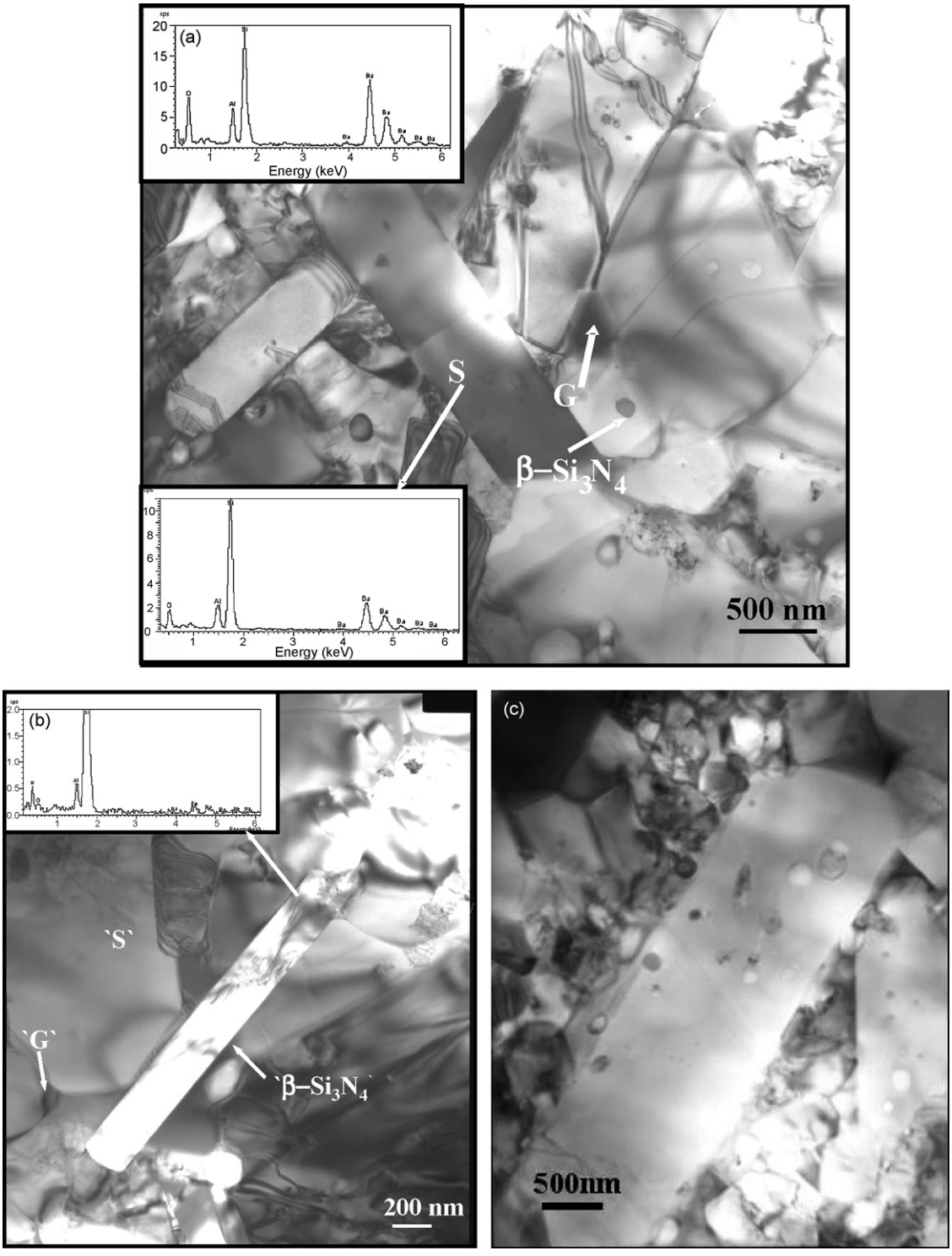

Fig. 2. Bright Field TEM image of S1700 ceramic (S-SiAlON, hot pressed at 1700 °C) detailing an overview of the microstructural phase evolution (a), the characteristic acicular β-Si_3N_4 grain (b) and the characteristic elongated S-phase SiAlON grain (c). Various characteristic phases, like 'S': S-phase, 'G': residual glass phase are indicated and the EDS spectra for the respective phases (top EDS spectrum in (a), acquired from the residual glass) are also shown in insets. Typical defect structure, consisting of a network of partial dislocations can be seen in (a). The spherical particles, contained within the S-phase crystal in (c) are Si_3N_4 phase.

of (8.5–8.9) × 10^5 cm/s, depending on the hot pressing temperature.

As can be noticed from Table 2, the apparent hardness varies over a range of 8.6–16 GPa at varying loads of 50–300 N for all the three investigated materials. A hardness vs. load curve, plotted in Fig. 4a reveals that the apparent hardness modestly increases with indent load, irrespective of the hot pressing temperature. However, the error bars associated with each measurement at higher load regime of 100 N or more, overlaps. Nevertheless, the apparent hardness data do show an increasing

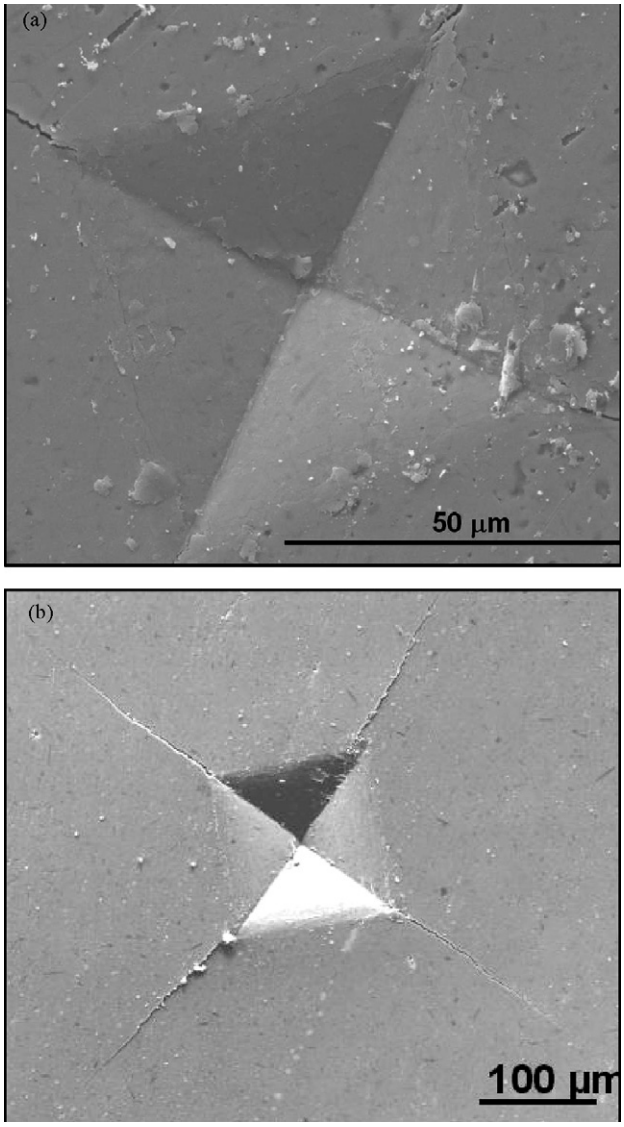

Fig. 3. SEM topography images of the Vickers indents and indentation-induced radial crack pattern in the Ba-S-SiAlON ceramic, hot pressed at 1750 °C and indented at varying loads: 100 N (a) and 300 N (b).

trend with indent load, which can be considered as the reflection of the reverse indentation size effect (RISE) behavior.[18,22] Among three of the materials, relatively higher apparent hardness (except at 200 N indent load) has been measured for S1750 and this can be ascribed to the reduced glassy phase along with the fully developed microstructural phases. In contrast to normal Indentation size effect (ISE), under the effect of RISE, material undergoes relaxation, which involves a release of the indentation stress along the surface away from the indentation site, which may be because of crack formation, dislocation activity, and/or elastic deformation of the tip of the indenter.[18,22] Keeping this in view, it is reasonable to argue that at low load, the dislocation plasticity can lead to more deformation and therefore, leads to reduced hardness in S-SiAlON material. At this point, it can be noted that the indentation response at higher load involved cracking.

It is to be emphasized here that the RISE has been reproduced after several careful measurements on various samples, taken from the same hot pressed disc. Since such behavior is reproducible on multiple indentation measurements, we are inclined to believe that such behavior is representative of true material behavior and cannot be attributed to any measurement artifact. It is therefore interesting to analyze the RISE behavior in the presence of complex microstructure in these three samples, while indenting at macro-load. It can be mentioned here that the RISE is observed at very low load (during micro- and nano-indentation) and reported for some semiconductors, like Si (1 1 1), GaAs (1 0 0), GaP (1 1 1), InP (1000), etc.[22–26] Also, the characteristic RISE phenomenon is reported for other covalently bonded ceramic, e.g. TiCN-based cermets with varying TiCN grain sizes at low load regime (1.47–40.67 N).[27] However, any comparison with RISE behavior of S-SiAlON with competing SiAlON ceramics is not possible, since only single hardness data is commonly reported for various developed SiAlON materials in the available literature. However, our study indicates that the complete description of the hardness properties requires the evaluation of hardness at varying indent loads.

Fig. 5, a plot of fracture toughness against crack length reveals some interesting observations about the crack growth resistance of Ba-doped S-SiAlON of material with increasing indent load (50–300 N). It can be noted from Fig. 5 that for S1600, toughness is low at small indent load and relatively higher toughness values are measured at 200 N or higher. It reaches an almost steady state toughness value of 5.5–5.9 MPa $m^{1/2}$ (flat R-curve). The relatively lower steady state toughness of S1600 can be attributed to the presence of a considerable amount of unreacted silicon nitride phase, as can be clearly noticed in Fig. 1a. In contrast, a sharp increase in toughness from 8.5 to 11.1 MPa $m^{1/2}$ with negligible increase in crack length (on increasing indent load from 200 to 300 N) has been experienced by S1700. More

Table 1
The detailed indentation data including, the crack length (l), indent diagonal length ($2a$) as well as the indentation toughness data for the hot pressed S-SiAlON ceramics

Material	Load								
	100 N			200 N			300 N		
	l (μm)	a (μm)	l/a	l (μm)	a (μm)	l/a	l (μm)	a (μm)	l/a
S1600	–	61.0	–	275.0	81.0	3.4	376.0	93.6	4.0
S1700	135.0	55.5	2.4	201.0	83.5	2.4	206.0	94.5	2.2
S1750	84.0	57.0	1.5	137.0	81.0	1.7	191.0	95.5	2.0

A maximum of 15% variation in the reported data has been measured.

Table 2
Summary of the mechanical properties of S-SiAlON, hot pressed at 1600 °C (S1600), 1700 °C (S1700) and 1750 °C (S1750), when subjected to indentation at varying indent load of 100 N, 200 N and 300 N

Material	Density (gm/cm^3)	E (GPa)	Indentation load at 50 N		Indentation load at 100 N		Indentation load at 200 N		Indentation load at 300 N	
			H_v (GPa)	K_{Ic} (MPa m$^{1/2}$)	H_v (GPa)	K_{Ic} (MPa m$^{1/2}$)	H_v (GPa)	K_{Ic} (MPa m$^{1/2}$)	H_v (GPa)	K_{Ic} MPa m$^{1/2}$
S1600	3.62	215	8.6 ± 0.1	2.4 ± 0.2	12.6 ± 0.8	–	13.7 ± 0.9	5.9 ± 0.03	16.0 ± 2.0	5.5 ± 0.3
S1700	3.63	228	12.7 ± 0.4	3.9 ± 0.3	15.1 ± 1.3	7.4 ± 0.2	13.2 ± 0.8	8.5 ± 0.3	15.5 ± 0.2	11.1 ± 0.6
S1750	3.65	212	12.5 ± 0.4	3.7 ± 0.1	14 ± 0.7	11.6 ± 0.6	14.1 ± 1.0	12.0 ± 0.8	15.3 ± 1.8	11.6 ± 0.2

The indentation data for 50 N load has been taken from Ref. 17.

importantly, a systematic increase in K_c from 3.7 to 11.6 MPa m$^{1/2}$ with increasing crack length (rising R-curve behavior) has been measured in S1750. From Fig. 5, it should therefore be clear that the pronounced 'R-curve' behavior (systematic increase in toughness with crack extension) is exhibited both by S1700 and S1750 ceramic, over the crack length of up to 200 μm. In particular, very stable R-curve behavior and better toughness property can be confirmed for S1750 ceramic.

4. Discussion

4.1. Load-dependent hardness property

Here, we make an attempt to explain the RISE effect from the fundamental indentation theory. In addition to a plastically deformed zone beneath the indenter, the indentation, taken at any given indent load of larger than a critical load, causes cracking in case of brittle ceramics. The indentation energy is generally partitioned to the plastic deformation and fracturing process of the indented material. At higher load, the effect of friction, surface roughness, strain gradient plasticity and the elastic recovery effects can be neglected in comparison to plastic deformation and fracture. In case of indentation cracking, the apparent hardness (H_{app}) measured by a Vickers diamond indenter can be analytically assessed[25,26];

$$H_{app} = \lambda_1 k_1 \left(\frac{P}{a^2}\right) + k_2 \left(\frac{P^{5/3}}{a^3}\right) \quad (2)$$

where 'a' is the indentation diameter, P is the indent load and λ_1, k_1 and k_2 are constants.

For a perfectly brittle solid

$$\lambda_1 = 0 \text{ and } H_{app} = K_2 \left(\frac{P^{5/3}}{a^3}\right) \quad (3)$$

After analyzing a larger number of experimentally measured hardness data (0.4–22 GPa), Sangwal[23] proposed a modified relationship:

$$H_v = K \left(\frac{P^{5/3}}{a^3}\right)^m \quad (4)$$

In the above expression, both K and m are constants and the value of 'm' is reported to be around 0.5–0.55.[24] Although the deformation dominated the hardness response at lower load, the observation of indent-induced radial cracking has been made at intermediate and higher loads. In order to critically analyze our experimental data, the measured apparent hardness values are plotted against ($P^{5/3}/a^3$) on log-scale, in Fig. 4b. It is clear from Fig. 4b that the measured data can be fitted closely with the linear correlation and the value of 'm' in the present case, is recorded to be 0.494, which is similar to earlier report.[24] However, the deviation in case of S1700 ceramic is more from the linear correlation (obvious from the corresponding hardness data), as it does not show the monotonically increase in hardness. Here, it needs to be emphasized that earlier RISE effect was observed at extremely low loads (<1 N)[22–24] and in case of TiCN cermets at indent load of less than 40 N.[27] But in the present case, such

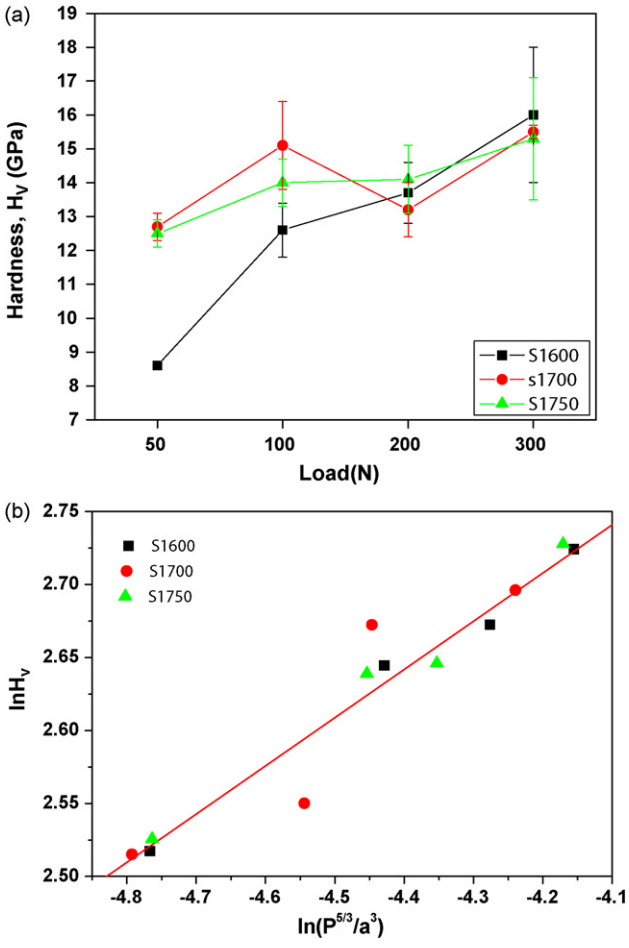

Fig. 4. Plot of hardness vs. load (a) and ln H_v against ln ($P^{5/3}/a^3$) (b), illustrating the reverse indentation size effect (RISE), exhibited by the S-SiAlON ceramics, when indented with a varying load of 50–300 N.

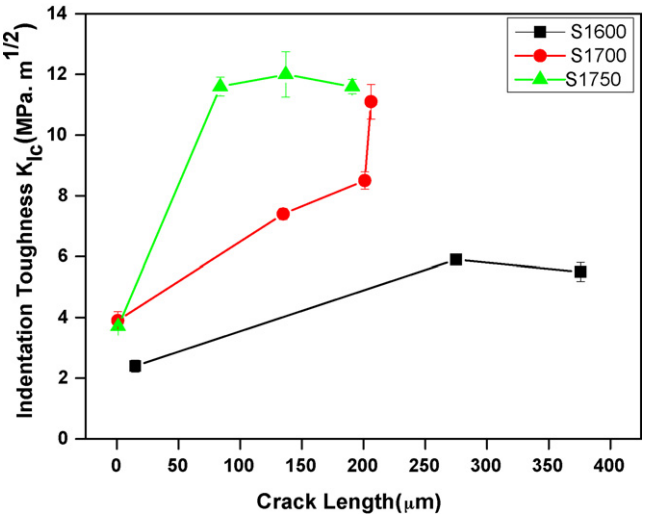

Fig. 5. Plot of indentation toughness vs. crack length for investigated S-SiAlON ceramics. A characteristic and a systematic increase in fracture toughness can be noted for all the investigated S-SiAlON ceramics.

effect is importantly observed at macro-loads (>50 N). This is an interesting and a new observation, which has ever been made on a structural ceramic.

From the above analysis, it is clear that the variation of apparent hardness with load can be attributed to the change of cracking behavior of the materials, which is ultimately controlled by the resultant microstructures evolved during hot pressing. It is obvious that the microstructural features are such that the cracking behavior is different at lower and higher load. At lower load, the plastic deformation is predominant and as a result much of the indentation energy is consumed for material flow and displacement, which lowers the apparent hardness. Whereas at higher load, the cracking is more predominant compared to the plastic deformation and consequently relatively more energy is consumed for crack initiation and propagation. This is supported by the abrupt change of l/a ratio from lower to higher load. In fact, the variation of (l/a) with the load is indicative of the dominance of the cracking over deformation and also an indirect measure of the partitioning of the relative energy for cracking and deformation. The evolution of complex distribution of microstructure eventually controls the crack initiation and propagation. In case of S1700 and S1750 ceramics, the RISE effect is less dominant and this can be attributed to the less availability of the glassy phases. However, the effect of RISE is still present. The effect of RISE is much more in S1600 ceramic sample than the other two samples. This also needs to be understood in the presence of a large amount of unreacted silicon nitride phase, as observed in dark contrast in Fig. 1a. It is also clear from the present investigation that effective area of contact (A) does not change significantly, but the length of the cracks (l) changed significantly and as a result, the apparent hardness increases ($H = P/A$) as applied load, P is increasing (see Tables 1 and 2). The nature of crack nucleation and propagation appears to be dependent on load. This essentially points out to the fact that cracking and deformation at lower load is somewhat different from that at higher load. It also implies that the relative energy distribution for deformation and fracturing is different at lower and higher load.

4.2. R-curve behavior

In assessing the toughness data, the results presented in Tables 1 and 2 as well as Fig. 5 need to be considered. The data presented in Table 2 and Fig. 5 reveal some of the interesting observations implicating strong dependence of the fracture toughness on the microstructural phase assemblage.

It needs to be mentioned here that R-curves are reported to be evaluated from Vickers indentation cracks for many of the structural ceramics, including alumina,[28] Y-TZP,[29] Si_3N_4,[30] SiC-based materials.[31] Although the use of indentation technique to assess the R-curve behavior of structural ceramics has been cautioned in a recent review article[32]; nevertheless, it has been reported that R curves, determined from indentation cracks follow closely with those evaluated from double cantilever beam (DCB) technique, in case of silicon nitride.[33] Similar result has been obtained for alumina ceramics.[34]

From Fig. 5, R-curve behavior of S-SiAlON ceramic can be assessed in terms of three aspects (a) initiation toughness (K_0), (b) steady-state toughness and (c) characteristic bridging length (l_c), i.e. the crack length increment over which K_0 attains steady-state toughness values. Now, as far as the hot pressing temperature is concerned, S-SiAlON, sintered at 1600 °C has the lowest K_0 and the K_0 of higher temperature sintered ceramics are comparable. In terms of steady-state toughness, similar trend is observed. As far as the third aspect is concerned, the characteristic bridging length for S1600 is 97 μm, while that for S1750 and S1750 ceramic is around 200 μm.

In order to further understand the operating toughening mechanisms, the interaction of the propagating crack with the microstructure has been studied in the SEM-BSE imaging mode (see Fig. 6). A typical, not representative though, case of multiple indentation cracking has been chosen to provide evidences of important aspects of crack–microstructure interaction. Various observations can be summarized as (a) sinusoidal trajectory/tortuous crack path (see upper crack) indicating enhanced crack growth resistance, (b) evidences of grain bridging and pull out and (c) frequent occurrence of debonding of elongated S-phase grains in the crack wake. Similar crack–microstructure interaction is commonly reported for various SiAlON ceramics.[2,8] The increased resistance offered by the matrix of S1700/S1750 to the propagating crack, i.e. rising R-curve behavior, is therefore ascribed to the contribution made by elongated S-phase grains and whisker like β-Si_3N_4 grains through crack deflection and crack bridging respectively. In order to show detailed morphology of S-phase, a bright field TEM image of a single grain of platelet shaped S-phase has been demonstrated in Fig. 2c. The large aspect ratio of interlocking S-phase grains (Fig. 2a and c), in combination with the acicular β-Si_3N_4 needles, creates the possibilities for development of further toughening mechanisms, such as frictional and mechanical interlocking between the separated fracture surfaces by deflecting the crack. This can occur simultaneously with β-Si_3N_4 needles dissipating considerable strain energy through

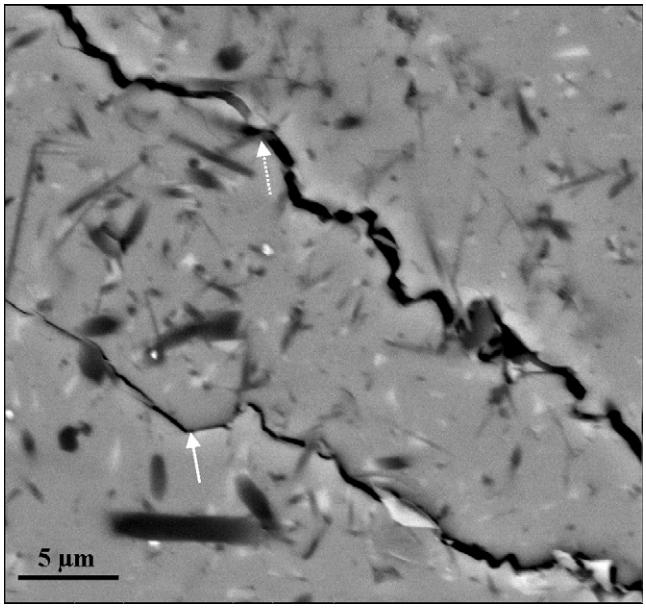

Fig. 6. SEM image illustrating crack–microstructure interaction in S1750 ceramic. While the single pointed arrow indicates typical crack-S phase interaction, the dotted arrow indicates the pull out of β-Si_3N_4 needles.

friction, generated by their motion against the matrix during elastic stretching along the debonded interface and pull out. Therefore, more energy is needed for separation of the fractured surfaces, which in macroscopic terms appears as the increased toughness.

From the above observations, it is clear that crack bridging and grain pullout, both contribute to moderately high toughness of Ba-S-SiAlON ceramic. We now analyze this observation in the light of a reported model, which correlates the fracture resistance with microstructure, containing elongated ceramic grains.[28] Such a model is useful to predict the frictional work, which is the main source of fracture energy. Also, the near tip toughening phenomenon, e.g. elastic bridging due to grain bonding is ignored. Another assumption is that the decohesion of an elongated/platelet shaped grain, prior to pull out, preferably occurs along the grain boundary by intergranular fracture. On the basis of the above assumptions, Becher et al.[35] arrived at the following expression correlating fracture toughness (K) with the microstructural features:

$$K = C\sqrt{\sum_i V_i W_i (\mathrm{AR}_i)^2} \tag{5}$$

In the above expression, V is volume fraction of elongated grains, W is grain width, 'AR' is the aspect ratio of elongated grains and the suffix 'i' denotes a group of ith type of elongated grains. Also, the value of 'C' for different elongated phases are taken as same.

Since the presently investigated Ba-doped S-SiAlON ceramics characteristically contain two types of elongated phases: S-phase and β-Si_3N_4 needles; Eq. (5) can be appropriately adapted as:

$$K = C\sqrt{V_s W_s (\mathrm{AR}_s)^2 + V_\beta W_\beta (\mathrm{AR}_\beta)^2} \tag{6}$$

where the suffix 's' and 'b' denotes the S-phase and β-Si_3N_4, respectively. Following the original model,[35] the fitting parameter/constant 'C' in Eq. (5) or (6), can be expressed as

$$C = \sqrt{\frac{E\tau}{6(1-\nu^2)}} \tag{7}$$

In the above expression, E is elastic modulus, ν is Poisson's ratio and τ is interfacial friction. It is also clear from Eqs. ((5) and (7)) that the aspect ratio of elongated phase, in comparison with width or volume fraction, should have more influence on the toughness.

In the present case, we have considered the microstructural data and mechanical property values of S1700 sample, to illustrate how the above-mentioned toughening model can be appropriate for S-SiAlON ceramic. Average aspect ratios (AR) of 3.44 and 7.0 and widths (W) of 1.14 and 0.57 μm for S-phase grains and β-Si_3N_4, respectively were considered in our calculation (also mentioned in Section 3.1). Considering the fact that 85% ($V_s = 0.85$) S-phase grains and 9% of β-Si_3N_4 needles ($V_\beta = 0.09$) are present in the investigated microstructure, the value of interfacial friction (τ) from Eqs. (6) and (7) has been computed to be 203.8 MPa. In our calculation, ν is taken as 0.3 and the toughness measured at 300 N load ($K = 11.1\ \mathrm{MPa\,m^{1/2}}$) was considered. It can be mentioned here that Chen and co-workers, using the identical model, estimated τ of 108 MPa in case of α-SiAlON materials (elongated grain morphology).[3] It has also been commented that the first term in the right hand side of Eq. (5) is rather a constant and does not depend on compositional aspect, to any significant extent.[3] Therefore, our calculation provides estimates of interfacial friction (τ) for S-SiAlON ceramics, which is in reasonable agreement with other SiAlON ceramic having similar grain morphology. It needs to be mentioned here that the possibility of grain pull out at an inclined angle was not considered in the above model.

It is also important to assess how the mechanical properties of S-SiAlON ceramic are comparable with the existing SiAlONs. Like many other ceramics, the properties of various SiAlON ceramics is strongly sensitive to microstructural characteristic, in particular grain shape/aspect ratio, intergranular phase, amount of seed crystals, ratio of α to β phases, etc. (e.g. see Refs. 35,37–39). Table 3 presents the summary of the mechanical property data of some selected SiAlON ceramics and such data illustrate a large variation in apparent hardness and toughness properties. Such a broad spectrum of properties can be uniquely described by two end members, i.e. the equiaxed α-SiAlON material with combination of high apparent hardness ($H_{V10} = 22$ GPa) and low toughness ($K_c = 3\ \mathrm{MPa\,m^{1/2}}$),[11] and β-SiAlON ceramic with high toughness (>6 $\mathrm{MPa\,m^{3/2}}$), imparted by needle like β-Si_3N_4 grains and low hardness (∼15 GPa). The advantages associated with the two phases have been utilized in the development of "in situ self-reinforced multiphase α–β structure". However, the optimization of the fracture toughness has been found to be at the expense of high hardness of α-grain matrix.[8,13] This fact led to the development of "single phase in situ toughened α-SiAlON", wherein the

Table 3
A comparative study of the S-SiAlON ceramic, hot pressed at 1750 °C with previously investigated competing Si_3N_4-based materials, in terms of hardness and indentation toughness properties

Sl. No.	Material under study	Starting material and/or method of fabrication	Hardness H_{v10} (GPa)	Fracture toughness K_c (MPa m$^{1/2}$)	Reference
1	Y-α SiAlON ($Y_{0.5}Si_{9.3}Al_{9.3}O_{1.2}N_{14.8}$)	α-Si_3N_4, AlN, Al_2O_3, Y_2O_3: HP at 1900 °C for 1 h, in N_2	21.0	12.0	2,3
2	Nb-stabilized α-SiAlON	β-Si_3N_4, AlN, Al_2O_3, Si_3N_4: HP at 1950 °C and heat treated for 12 h at 1650 °C	21.7	6.3	11
3	Lu + 5% Lu_2SiO_5	α-Si_3N_4, Al_2O_3, AlN, SiO_2, Lu_2O_3: HP at 1950 °C for 2 h in N_2	18.9	4.4	42
4	Dy-α SiAlON	α-Si_3N_4, AlN, Al_2O_3, Dy_2O_3: PLS at 1800 °C and then GPS at 1900 °C for 1 h	18.8	6.3	6
5	Y-α SiAlON	By post-sintering the nitrided compact at 1900 °C for 3 h.	18.5	5.1	4
6	Si_3N_4 + 20 vol% (9:1 AlN/Y_2O_3)	α-Si_3N_4, with 20% AlN, Al_2O_3, AlN:Y_2O_3 in 9:1 molar ratio: GPS at 1900 °C, 2 h in N_2	18.5	5.1	5
7	Y-Yb-α-SiAlON	α-Si_3N_4, AlN, (Y,Yb)O_3: HP at 1600–1750 °C in vacuum	18.9	4.6	42
8	Si_3N_4	HIPed Si_3N_4 + MgO	17.0	6.0	40
9	S-SiAlON	α-Si_3N_4, AlN, Al_2O_3, $BaCO_3$: HP at 1750 °C, 2 h in N_2 atmosphere	14.0	11.6	Present work
10	β-SiAlON	$Si_{6-z}Al_zO_zN_{8-z}$, $z = 0.3$	15.5	4.7	43
11	(Ce–Y) α-SiAlON	α-Si_3N_4, AlN, Al_2O_3 with CeO_2 (SHS-ed) CeO_2:Y_2O_3 in 1:0:0.375 molar ratio: HP at 1750 °C, for 1 h in N_2	15.2	4.9	6
12	α-SiAlON–10%β–SiAlON	α-SiAlON 76.92 wt% Si_3N_4, 13.46 wt% AlN, 5.77 wt% Y_2O_3, 3.85 Al_2O_3, reinforced with 10% β-SiAlON fiber	14.8	5.9	41
13	α-SiAlON (Equiaxed)	Starting powders α-Si_3N_4, Al_2O_3, AlN and Y_2O_3	22.0	3.0	11
14	Y_2O_3–Si_3N_4	Hot pressed (1650 °C, 1 h)	15.2	7.1–8.1	37
15	Yb_2O_3–Si_3N_4	Hot pressed (1650 °C, 1 h)	13.9	7.4–8.5	37

Different processing routes mentioned are HP: hot pressed, PLS: pressure less sintering, HIP: hot isostatic pressing, GPS: gas pressure sintering, SHS: self-propagating high temperature synthesis.

coarse elongated α-SiAlON grains exhibit self-reinforcement and thus result in improved toughness without impairing the high hardness of α-SiAlON matrix.[8] Although, the toughness of S1750 (11.6 MPa m$^{1/2}$) is much higher than several Si_3N_4-derived ceramics;[6,8,12] the apparent hardness of S-SiAlON (hot pressed at 1750 °C), 15.3 GPa is much lower than many of the Si_3N_4-based ceramics, possessing elongated α-SiAlON grain morphology.[5,8,13] Nevertheless, the hardness properties of Ba-doped S-SiAlON are comparable or modestly better than some competing silicon nitrides.[37]

In summary, the investigated S-SiAlON ceramic represents a new class of SiAlON material, which offers important combination of *E*-modulus (more than 200 GPa), apparent hardness (up to 16 GPa) and toughness (up to 12 MPa m$^{1/2}$) property. In addition, this new material is different from many of the earlier developed SiAlONs, as they exhibit both increased apparent hardness and toughness property with indentation load or contact pressure. It can be pointed out here that R-curves are exhibited by a wide range of SiAlON materials, e.g. Y-α-SiAlON,[2] in situ toughened Y-α–SiAlON, Ca-α-SiAlON,[39] etc. Depending on the amount of seed crystals, a peak toughness of 10 MPa m$^{1/2}$ or little higher was recorded in these ceramics.

In view of the above observations, we believe that S-SiAlON ceramics can be considered for structural application, provided the combination of hardness and toughness property can be further boosted up by microstructural tailoring, for example, by incorporating Si_3N_4 seeds. To this end, an optimal balance of the amount of elongated S-phase grains and β-Si_3N_4 phase is required. Also, the presence of low amount of glass phase in S-SiAlON ceramic can be beneficial from the perspective of high temperature structural application. Future attempts can be made to crystallize the residue glass of S-SiAlON ceramic and thereafter, assessing the changes in mechanical properties. As an additional note, it can be mentioned here that our recent tribological study on one of the investigated Ba-doped S-SiAlON ceramic (S1750) reveal friction and wear properties, which are comparable with competing SiAlON ceramics. More details can be found elsewhere.[36] In view of the above observations, it can be stated that the newly developed Ba-doped S-SiAlON ceramic can be considered as a potential competitive SiAlON composition for various engineering applications.

As an additional point of consideration, it needs to be mentioned here that although hot pressing has been largely used in the fabrication of SiAlON samples in research laboratories, the gas pressure sintering with nitrogen gas or sinter-HIPing are the better processing approaches to investigate the industrial scale feasibility for the production of nitride ceramics, like α-SiAlON ceramics. Such experiments with S-SiAlON ceramics are planned in our future investigation.

5. Conclusions

Based on the present investigation it can very well be concluded that hot pressed S-SiAlON, has shown rather promising results in terms of mechanical properties, when compared with other SiAlON ceramics. This optimization of the properties can be attributed to the fully developed and stabilized microstructure, consisting of elongated S-phase grains along with the presence of acicular β′ grains and less amount of glass residue at triple junctions/grain boundaries. The salient points, that emerge from this study include:

(a) The mechanical property evaluation using Vickers indentation at varying indent loads (up to 300 N) reveals load dependent apparent hardness and fracture toughness of S-SiAlON ceramic, hot pressed in the range of 1600–1750 °C. The apparent hardness broadly increases with indent load, irrespective of processing temperature. The apparent hardness values recorded at 300 N indent load vary in the range of 15–16 GPa, depending on hot pressing temperature.
(b) Careful analysis of the indentation data reveals the reverse indentation size effect (RISE) in all S-SiAlON samples. The RISE effect has been attributed to the predominance of cracking over deformation at higher load, resulting in an increase in apparent hardness compared to that at lower load. The interplay between cracking and deformation has been explained based on the complex microstructures evolved during hot pressing.
(c) An important result has been that the hot pressed S-SiAlON ceramics exhibit pronounced R-curve behavior, i.e. a systematic increase in toughness with increase in crack length. A maximum toughness of 11–12 MPa $m^{1/2}$ was obtained in case of S-SiAlON hot pressed at 1750 °C. The increased toughness can be ascribed to noticeable contribution from crack deflection, crack bridging, and crack branching, imparted by elongated S-phase grains as well as β-Si_3N_4 needles. Based on the assessment of hardness and toughness properties, it is clear that higher hot pressing temperature of 1750 °C is the optimal sintering condition and such processing temperature is much less than many of the α-SiAlON ceramics.
(d) As far as the crack–microstructure interaction is concerned, the use of a theoretical toughening model based on predominant toughening by platelet shaped S-phase grains as well as contribution from the β-Si_3N_4 needles provided an estimate of the interfacial friction of around 200 MPa, which is in reasonable agreement with other competing SiAlON ceramics.

Acknowledgements

One of the authors (BB) wishes to thank Department of Science and Technology, Government of India for 'BOYCAST' fellowship. The authors also thank Prof. Rajendra K. Bordia for fruitful discussions during the manuscript preparation.

References

1. Kurama, S., Herrmann, M. and Mandal, H., The effect of processing conditions, amount of additive and composition on the microstructures and mechanical properties of α-SiAlON ceramics. *J. Eur. Ceram. Soc.*, 2003, **22**, 109–119.
2. Zenotchkine, M., Shuba, R., Kim, J.-S. and Chen, I.-W., Effect of seeding on the microstructure and mechanical properties of alpha-SiAlON: I, Y-SiAlON. *J. Am. Ceram. Soc.*, 2002, **85**(5), 1254–1259.
3. Zenotchkine, M., Shuba, R. and Chen, I.-W., Effect of seeding on the microstructure and mechanical properties of alpha-SiAlON. III. Comparison of modifying cations. *J. Am. Ceram. Soc.*, 2003, **86**, 1168–1175.
4. Kaga, Y., Jones, M. I., Hirao, K. and Kanzaki, S., Fabrication of elongated α-SiAlON via a reaction-bonding process. *J. Am. Ceram. Soc.*, 2004, **87**(5), 956–959.
5. Santos, C., Strecker, K., Rebeiro, S., de Souza, J. V. C., Silva, O. M. M. and da Silva, C. R. M., α-SiAlON ceramics with elongated grain morphology using an alternative sintering additive. *Mater. Lett.*, 2004, **58**, 1792–1796.
6. Jiang, J., Wang, P., He, W., Chen, W., Zhuang, H., Cheng, Y. *et al.*, Study on the stability of Ce α-SiAlON derived from SHS-ed powder. *J. Eur. Ceram. Soc.*, 2004, **24**, 2853–2860.
7. Santos, C., Ribeiro, S., Daguano, J. K. M. F., Rogero, S. O., Strecker, K. and Silva, C. R. M., Development and cytotoxicity evaluation of SiAlON ceramics. *Mater. Sci. Eng. C*, 2007, **27**, 148–153.
8. Mandal, H., New developments in α-SiAlON ceramics. *J. Eur. Ceram. Soc.*, 1999, **19**, 2349–2350.
9. Turan, S., Kara, F. and Mandal, H., Transmission electron microscopy of SrO containing multi-cation doped α-SiAlON ceramics. *Mater. Sci. For.*, 2002, **383**, 37–42.
10. Acikbas Calis, N., Suvaci, E. and Mandal, H., Fabrication of functionally graded SiAlON ceramics by tape casting. *J. Am. Ceram. Soc.*, 2006, **89**(10), 3255–3257.
11. Wei-Chen, I. and Rosenflanz, A., A tough SiAlON ceramic based on α-Si_3N_4 with a whisker like microstructure. *Nature*, 1997, **389**, 701–704.
12. Ye, F., Michael, Hoffmann, J., Holzer, S., Zhou, Y. and Iwasa, M., Effect of amount of additives and post heat treatment on the microstructure and mechanical properties of Yttrium α-SiAlON ceramics. *J. Am. Ceram. Soc.*, 2003, **86**(12), 2136–2142.
13. Zhang, C., Komeya, K., Tatami, J. and Meguro, T., Inhomogeneous grain growth and elongation of Dy-α-SiAlON ceramics at temperatures above 1800 °C. *J. Eur. Ceram. Soc.*, 2000, **20**, 939–944.
14. Hwang, C. J., Susintzky, D. W. and Beaman, D. R., Preparation of multication α-SiAlON containing strontium. *J. Am. Ceram. Soc.*, 1995, **78**(3), 588–592.
15. Esmaeilzadeh, S., Grins, J., Shen, Z., Eden, M. and Thiaux, M., Study of SiAlON S-phases $M_2Al_xSi_{12-x}N_{16-x}O_{2+x}$, M: Ba and $Ba_{0.9}Eu_{0.1}$, by X-ray single crystal diffraction, X-ray powder diffraction, and solid-state nuclear magnetic resonance. *Chem. Mater.*, 2004, **16**(11), 2113–2120.
16. Shen, Z., Grins, J., Esmaeilzadeh, S. and Ehrenberg, H., Preparation and crystal structure of a new Sr containing SiAlON phase $Sr_2Al_xSi_{12-x}N_{16-x}O_{2-x}$ (x~2). *J. Mater. Chem.*, 1999, **9**, 1019–1022.
17. Basu, B., Lewis, M. H., Smith, M. E., Bunyard, M. and Kemp, T., Microstructure development and properties of novel Ba-doped S-phase SiAlON ceramics. *J. Eur. Ceram. Soc.*, 2006, **26**, 3919–3924.
18. Krell, A., A new look at the influences of load, grain size, and grain boundaries on the room temperature hardness of ceramics. *Int. J. Refract. Met. Hard Mater.*, 1998, **16**, 331–335.
19. Niihara, K., Morena, R. and Hasselman, P. H., Evaluation of K_{Ic} of Brittle solids by the indentation methods with low crack to indent ratios. *J. Mater. Sci. Lett.*, 1982, **1**, 13–16.
20. Palmqvist, S., Occurrence of crack formation during Vickers indentation as a measure of the toughness of the hard materials. *Arch. Eisenhuttenwesen*, 1962, **33**, 629–633.
21. Mitomo, M. and Uenosono, S., Microstructural development during gas pressure sintering of alpha silicon nitride. *J. Am. Ceram. Soc.*, 1992, **75**, 103–108.

22. Mukhopadhyay, N. K. and Paufler, P., Micro-and nano-indentation techniques for mechanical characterization of materials. *Int. Mater. Rev.*, 2006, **51**(4), 209–245.
23. Sangwal, K., On the reverse indentation size effect and microhardness measurement of solids. *Mater. Chem. Phys.*, 2000, **63**, 145–152.
24. Sangwal, K. and Surowska, B., Study of indentation size effect and microhardness of $SrLaAlO_4$ and $SrLaGaO_4$ single crystals. *Mater. Res. Innovat.*, 2003, **7**, 91–104.
25. Li, H. and Bradt, R. C., The effect of indentation induced cracking on apparent microhardness. *J. Mater. Sci.*, 1996, **31**, 1065–1070.
26. Hays, C. and Kendall, E. G., An analysis of knoop microhardness. *Metallography*, 1973, **6**, 275–282.
27. Gong, J., Miao, H., Zhao, Z. and Guan, Z., Load-dependence of the measured hardness of Ti(C, N)-based cermets. *Mater. Sci. Eng.*, 2001, **A303**, 179–186.
28. Braun, L. M., Bennison, S. J. and Lawn, B. R., Objective evaluation of Short-crack toughness curves using indentation flaws: case study on alumina based ceramics. *J. Am. Ceram. Soc.*, 1992, **75**, 2049–2057.
29. Anderson, R. M. and Braun, L. M., Technique for the R-curve determination of Y-TZP using indentation technique. *J. Am. Ceram. Soc.*, 1990, **73**, 3059–3062.
30. Li, C. W., Lee, D. J. and Lui, S. C., R-curve and strength for in situ reinforced silicon nitrides with different microstructures. *J. Am. Ceram. Soc.*, 1992, **75**, 1777–1785.
31. Choi, R. and Salem, J. A., Strength, toughness and R-curve behavior of SiC Whisker-reinforced composite Si_3N_4 with reference to monolithic Si_3N_4. *J. Mater. Sci.*, 1992, **27**, 1491–1498.
32. Munz, D., What can we learn from R-curve measurements? *J. Am. Ceram. Soc.*, 2007, **90**(1), 1–15.
33. Li, C. W. and Yamanis, J., Super tough silicon nitride with R curves behavior. *Ceram. Eng. Sci. Proc.*, 1989, **10**, 632–645.
34. Cook, R. F., Liniger, E. R., Steinbrech, R. W. and Deuerler, F., Sigmoidal indentation strength characteristics of polycrystalline alumina. *J. Am. Ceram. Soc.*, 1994, **77**, 303–314.
35. Becher, P. F., Lin, H. T., Hwang, S. L., Hoffmann, M. J. and Chen, I.-W., The influence of microstructure on the mechanical behavior of silicon nitride ceramics. *Mater. Res. Soc. Symp. Proc.*, 1993, **287**, 147–158.
36. Manisha and Basu, B., Tribological properties of a hot pressed Ba-doped S-phase SiAlON ceramic. *J. Am. Cer. Soc.*, 2007, **90**(6), 1858–1865.
37. Zheng, Y. S., Knowles, K. M., Vieira, J. M., Lopes, A. B. and Oliveira, F. J., Microstructure, toughness and flexural strength of self-reinforced silicon nitride ceramics doped with yttrium oxide and ytterbium oxide. *J. Microsc.*, 2001, **201**, 238–249.
38. Deng, Z. Y., Inagaki, Y., She, J., Tanaka, Y., Liu, Y. F., Sakamoto, M. *et al.*, Long crack R-curve of aligned porous silicon nitride. *J. Am. Ceram. Soc.*, 2005, **88**(2), 462–465.
39. Zenotchkine, M., Shuba, R., Kim, J. S. and Chen, I. W., R-curve behavior of in situ toughened α-SiAlON ceramics. *J. Am. Ceram. Soc.*, 2001, **84**(4), 884–886.
40. Novak, S., Drazic, G., Samardija, Z., Kalin, M. and Vizintin, J., Wear of silicon nitride ceramics under fretting conditions. *Mater. Sci. Eng.*, 1996, **A215**, 125–133.
41. Reis, P., Venceslau Filho, J., Davim, P., Xu, X. and Ferreira, J. M. F., Wear behavior on advanced structural ceramics: α-SiAlON matrix reinforced with β-SiAlON fibers. *Mater. Des.*, 2005, **26**, 417–423.
42. Jones, M. I., Hyugab, H., Hirao, H. and Yamauchi, Y., Wear properties under dry sliding of Lu-α SiAlONs with in situ reinforced microstructures. *J. Eur. Ceram. Soc.*, 2004, **24**, 3581–3589.
43. Basu, B., Vleugels, J., Kalin, M. and Van Der Biest, O., Friction and wear behavior of SiAlON ceramics under fretting contacts. *Mater. Sci. Eng.*, 2003, **A359**, 228–236.